Journal of Power Sources 196 (2011) 9169–9175

Contents lists available at ScienceDirect

Journal of Power Sources

journal homepage: www.elsevier.com/locate/jpowsour

A microfabricated low cost enzyme-free glucose fuel cell for powering low-power implantable devices

Vlad Oncescu, David Erickson*

Sibley School of Mechanical and Aerospace Engineering, Cornell University, Ithaca, NY 14853, United States

ARTICLE INFO

Article history:
Received 12 June 2011
Received in revised form 29 June 2011
Accepted 30 June 2011
Available online 29 July 2011

Keywords:
Glucose fuel cell
Implantable device
Enzyme-free
Stacked electrode

ABSTRACT

In the past decade the scientific community has showed considerable interest in the development of implantable medical devices such as muscle stimulators, neuroprosthetic devices, and biosensors. Those devices have low power requirements and can potentially be operated through fuel cells using reactants present in the body such as glucose and oxygen instead of non-rechargeable lithium batteries. In this paper, we present a thin, enzyme-free fuel cell with high current density and good stability at a current density of 10 $\mu A\,cm^{-2}$. A non-enzymatic approach is preferred because of higher long term stability. The fuel cell uses a stacked electrode design in order to achieve glucose and oxygen separation. An important characteristic of the fuel cell is that it has no membrane separating the electrodes, which results in low ohmic losses and small fuel cell volume. In addition, it uses a porous carbon paper support for the anodic catalyst layer which reduces the amount of platinum or other noble metal catalysts required for fabricating high surface area electrodes with good reactivity. The peak power output of the fuel cell is approximately 2 $\mu W\,cm^{-2}$ and has a sustainable power density of 1.5 $\mu W\,cm^{-2}$ at 10 $\mu A\,cm^{-2}$. An analysis on the effects of electrode thickness and inter electrode gap on the maximum power output of the fuel cell is also performed.

1. Introduction

1.1. Internal power supplies for implantable devices

For over three decades, low-power implantable devices have been powered using non-rechargeable lithium batteries [1] that have a lifespan of 5–10 years for low-power drain devices such as pacemakers but can only operate for up to a year at power-densities above 45 $\mu W\,cm^{-3}$ [2]. Therefore alternative power sources are required for the long-term operation of the implantable devices currently being developed [3–10]. Although remote powering of implantable devices is in theory possible using transcutaneous energy transmission systems [11,12], in many situations it is desirable to develop autonomous implantable devices that do not require any external power input. Alternative approaches considered for internally powering autonomous implantable devices include: microbial and enzymatic bio fuel cells [13–16], abiotic fuel cells [17], thermal power sources [18] and vibrational energy convertors [19–21]. Abiotic glucose fuel cells [22–24] are promising because they offer reasonable performance and higher stability than enzymatic [25,26] and microbial glucose fuel cells [27,28]. Although they offer better stability, thermal power sources and vibration energy convertors have a theoretical power limit that is too low for many implantable devices currently under development.

1.2. Abiotically catalyzed glucose fuel cells

The ability of different abiotic catalysts to catalyze oxygen and glucose reactions has been extensively studied. It was demonstrated that several catalysts such as silver and activated carbon can selectively catalyze oxygen reduction in the presence of glucose while platinum alloys such as platinum–bismuth can catalyze glucose oxidation in deaerated solutions. To date, no abiotic catalyst material has been found to selectively catalyze glucose oxidation in the presence of oxygen [17]. In order to get around the catalyst selectivity issue, a stacked electrode approach has been used to achieve reactant separation [23,29]. In this approach, a permeable cathode that selectively catalyzes oxygen reduction is placed in front of the anode, thus removing some of the oxygen from the solution before it defuses to the anode allowing glucose oxidation to proceed at low oxygen concentrations. Porous cathodes have been fabricated either by suspending the cathode catalyst material in a hydro-gel and spreading the mixture onto a current conducting platinum mesh [29] or by etching holes through a silicon cathode support before depositing the catalyst layer [30]. Since the

* Corresponding author. Tel.: +1 607 255 4861; fax: +1 607 255 1222.
E-mail address: de54@cornell.edu (D. Erickson).

0378-7753/$ – see front matter © 2011 Elsevier B.V. All rights reserved.
doi:10.1016/j.jpowsour.2011.06.100

last approach does not require a conducting platinum mesh, it is more suited for fabricating highly compact electrodes. In order to increase the surface area of the electrodes, several methods such as Raney type alloying and coating of the silicon wafers with carbon nanotubes have been used [31].

In this paper we demonstrate the advantage of fabricating the cathode using a thin platinum catalyst layer deposited on a carbon paper membrane. Since the carbon paper is conductive, porous, and has a high surface area, the platinum catalyst layer can be deposited directly on the membrane thus requiring less platinum catalyst and less intermediate steps in order to obtain a high surface area electrode. Section 2 gives an overview of the theory behind abiotic glucose fuel cells and some important characteristics affecting performance for the stacked electrode design. Section 3 goes over the fabrication of the fuel cell presented in this paper, Section 4 describes the experimental setup and Section 5 presents the experimental results.

2. Abiotic glucose fuel cell theory and operation

Glucose fuel cells produce electrical current through a proton coupled electron transfer (PCET) reaction where oxygen is reduced at the cathode and glucose is oxidized at the anode. Assuming glucose is oxidized to gluconic acid, the theoretical cell voltage of a fuel cell is 1.3 V [17]. The open circuit voltage is however much lower than that due to fuel and oxidant cross-over resulting in mixed potentials at both electrodes. Cross-over occurs when both fuel and oxidant react at the same electrode, a situation that is unavoidable in glucose fuel cells operating in vivo where glucose and oxygen are hard to effectively separate before reaching the electrodes.

The stacked electrode design takes advantage of the fact that the physiological concentration of glucose is two orders of magnitude higher than that of dissolved oxygen [17]. Consequently most of the oxygen is reduced before crossing the porous cathode while only a small fraction of the glucose is oxidized. The glucose oxidation reaction can therefore proceed at the anode under low-oxygen conditions. In this manner, stacked electrode fuel cells can achieve good power output despite poor electrode selectivity. In order to reduce the amount of oxygen reaching the anode and competing with the glucose oxidation reaction, it is possible to increase the thickness of the cathode. However, we will show experimentally in Section 5.4 that this also reduces the maximum power output of the full cell by decreasing glucose diffusion to the anode.

When a small current is drawn from a fuel cell, the actual voltage is lower than the theoretical voltage due to activation losses. Activation losses depend on the nature of the catalyst and are significant in abiotic glucose fuel cells due to slow reaction kinetics at the electrodes. As the current is increased the cell voltage drops linearly due to ohmic losses in the fuel cell caused by the relatively poor conductivity of the electrolyte. The resistance of the electrolyte is given by:

$$R = \frac{L}{\sigma A} \tag{1}$$

where L is the distance between electrodes, σ is the electrical conductivity and A is the cross-sectional area of the electrolyte. From Eq. (1) it can be seen that increasing the gap between the electrodes increases the ohmic losses in the fuel cell. In addition, separating the electrodes by a porous filter membrane, as is commonly done, greatly decreases the electrolyte cross-sectional area and increases ohmic resistance [29]. In this paper, we have assembled the fuel cell without a filter membrane in order to avoid this problem.

Decreasing the inter-electrode gap also produces a higher glucose concentration gradient at the anode. The relationship between current density and the concentration gradient is given by:

$$\frac{i}{A} = nFD\frac{C_o - C_b}{\delta} \tag{2}$$

where i/A is the Faradaic current density, n is the number of electrons transferred, F is the Faraday constant, D is the diffusion coefficient and $(C_o - C_b)$ is the difference between the concentration at the electrode surface and the bulk concentration over the Nernst diffusion layer thickness δ. Fig. 1 shows the main sources of voltage losses that occur in glucose fuel cells as well as the change in glucose concentration through the inter-electrode gap.

Despite the positive effects of reducing the distance between electrodes, it is shown experimentally in Section 5.4 that the maximum power density actually decreases as the distance between electrodes decreases below a certain critical length. This occurs when inter-electrode gap length approaches the Nernst diffusion layer thickness and starts affecting the concentration gradient at the anode. Other issues affecting performance at small inter-electrode gaps include hydrogen bubble formation in the inter-electrode gap [32] and accumulation of reaction products, such as gluconic acid and hydrogen ions, at the anode surface [33] due to poor diffusivity through the membrane. The latter also affects the pH in the inter-electrode gap and has a large effect on the reaction rates at the electrodes.

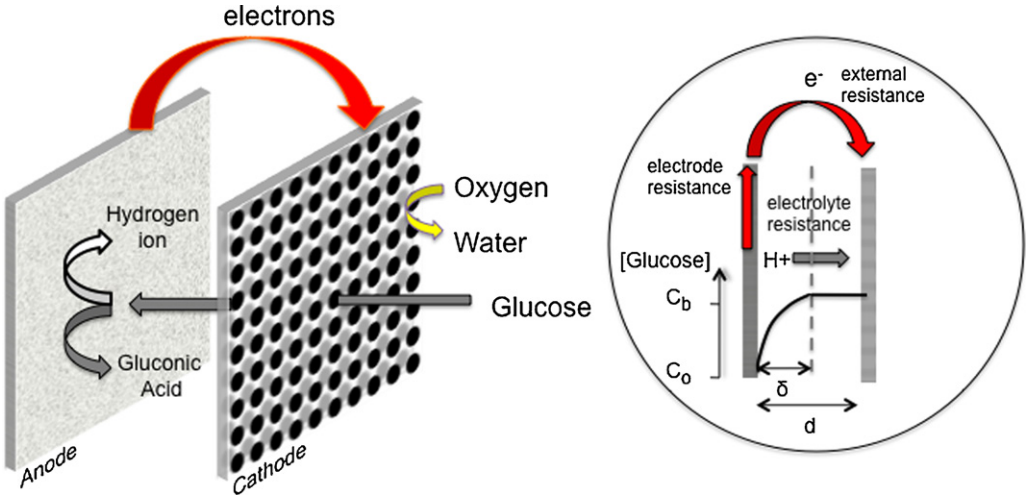

Fig. 1. Stacked glucose fuel cell structure with cell resistance losses and glucose concentration profile in the inter-electrode gap.

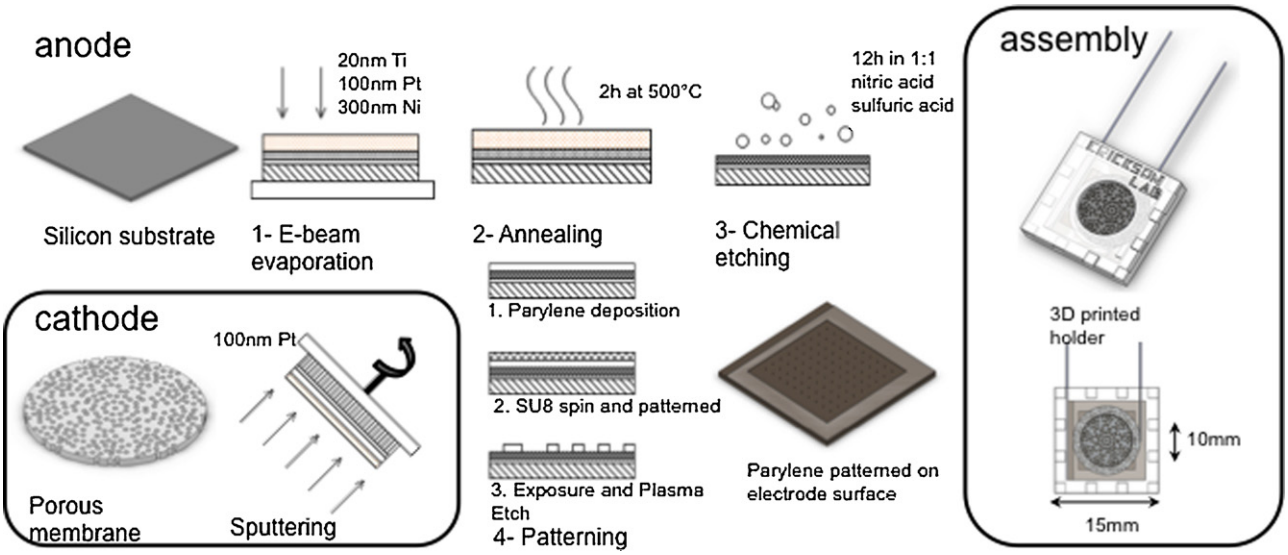

Fig. 2. Fabrication and assembly steps of the stacked electrode glucose fuel cell.

3. Fabrication

3.1. Anode fabrication

The steps for the anode microfabrication are shown in Fig. 2. A four inch silicon wafer was used as substrate for the catalyst layer deposition. High surface area Raney type anodes for glucose oxidation are obtained by alloying platinum with nickel and subsequently extracting the unalloyed nickel. It was demonstrated by Gebhardt et al. [31] that depending on the initial nickel to platinum ratio, such catalysts exhibit up to nine times higher current densities in deaerated phosphate buffer than conventional platinum black electrodes. E-beam evaporation (CHA Evaporator) was used to deposit 20 nm of titanium in order to promote adhesion followed by 100 nm of platinum and 300 nm of nickel. The wafer was subsequently annealed for 2 h in nitrogen gas at 500 °C (MRL Industries Furnace). In order to avoid oxide formation when opening and closing the furnace door, the stand-by temperature of the furnace was kept below 300 °C. The sheet conductivity of the wafer after each process step was measured using a CDE ResMap Resistivity 4 point Probe to ensure that no oxide layer would form at the surface and reduce the surface conductivity of the electrode. The wafers were then kept in 1:1 solution of sulfuric acid and nitric acid for 12 h in order to ensure that all the unalloyed nickel has been removed. Upon removal, X-ray photoelectron spectroscopy (XPS) analysis on the wafer was performed and it showed no traces of unalloyed nickel. The inter-electrode gap was patterned directly on the cathode using parylene for electrical insulation and SU-8 photo resist for setting the desired inter-electrode gap size. Approximately 2 μm of parylene was deposited using a Parylene Coating System. The SU-8 photoresist was then spun and patterned directly on top of the parylene. The patterned wafer was later diced in 15 mm by 15 mm squares using a K&S 7100 Dicing Saw. The parylene was then etched in oxygen plasma through the SU-8 mask using a Oxford PlasmaLab 80+ RIE System and the depth of the pattern was measured using a P-10 Profilometer tool.

3.2. Cathode fabrication

The cathode for oxygen reduction was fabricated by sputtering platinum directly onto a porous substrate. The porosity and structure of the support membrane has a strong effect on the amount of glucose and oxygen that passes through the cathode. Consequently several types of membranes were considered and two chamber diffusion experiments, not shown in this paper, were performed in order to characterize the diffusion through those membranes. Based on these experiments, Teflon coated carbon paper (Toray TGP-H-090) and anodized aluminum oxide membranes (Whatman AAO) were selected. Scanning electron microscope (SEM) images of the two membranes are presented in Fig. 3. The carbon paper membrane is 300 μm thick and has the advantage of being conductive and having a high surface area. The AAO membrane is non-conductive and has a relatively small surface area but has the advantage of being only 60 μm thick, which in principle allows for the fabrication of smaller more compact fuel cells with better glucose diffusion to the anode. The catalyst layer was obtained by directly sputtering 100 nm of platinum onto each side of the porous membranes. Better platinum coverage inside the pores was obtained when the porous membranes were rotated during deposition. Sections 5.1–5.3 present experimental results for fuel cells assembled using a carbon paper supported cathode, while Section 5.4 presents performance comparisons between fuel cells with carbon paper and AAO membrane supported cathodes.

3.3. Fuel cell assembly

Copper wires (28 Gauge L.J. Leahy) were bonded to the electrodes using silver epoxy (M.G. Chemicals). The electrodes were then held together in a specially designed 3D printed holder and epoxy (Hardman Double Bubble Epoxy) was used to seal the two parts of the holder together. Fig. 3 shows an assembled fuel cell mounted on a glass slide as well as scanning electron microscope (SEM) images of the anode and cathode surfaces.

4. Experimental setup and procedure

4.1. Fuel cell testing environment

All experiments were carried out under controlled conditions at physiological levels of glucose (5.0 mmol L^{-1}) and dissolved oxygen (7% saturation) in 0.01 M phosphate buffer saline (pH 7.4) at 37 °C using a setup similar to the one described by Kerzenmacher et al. [29] and presented here in Fig. 4a. Two flow meters (VWR 20–200 SCFM) were used to adjust the ratio of air and nitrogen (Airgas NI-200) flowing in the solution. In order to have a more stable environment and to minimize rapid changes in oxygen concentra-

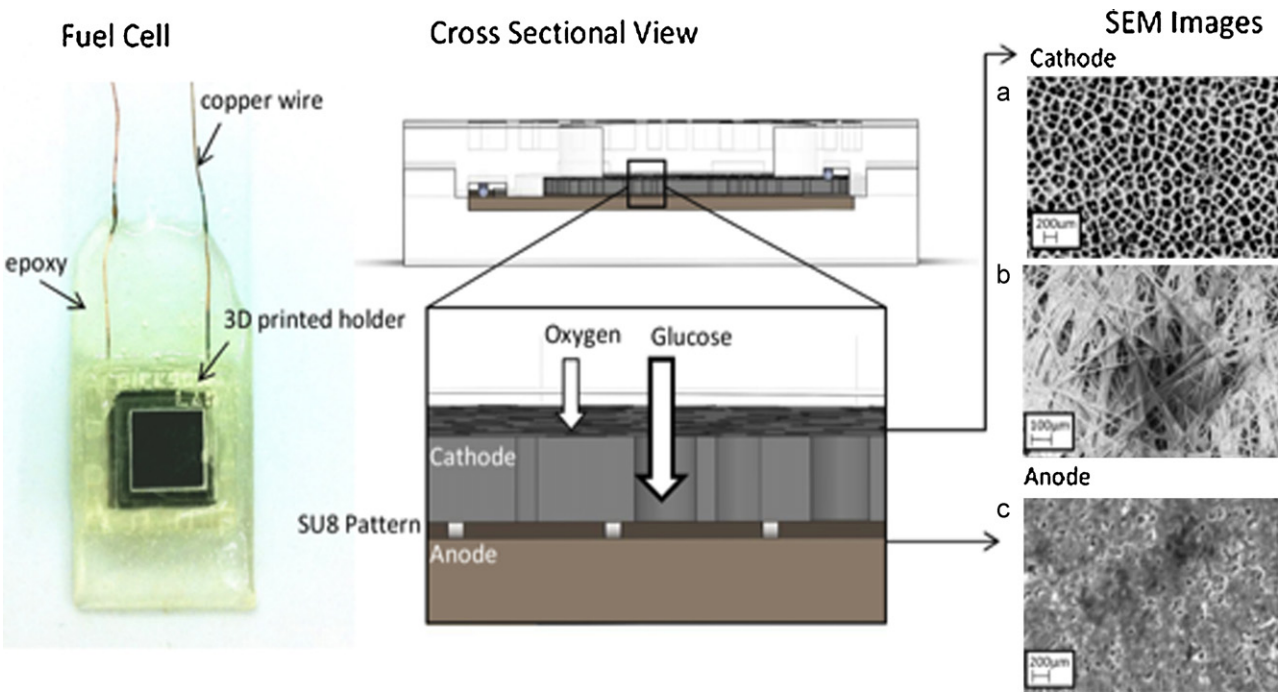

Fig. 3. Assembled fuel cell and SEM images of (a) AAO membrane cathode, (b) carbon paper porous cathode and (c) platinum–nickel alloyed anode.

tions, the testing chamber was divided in two parts: one where the fuel cells are kept and one where the nitrogen and glucose are introduced. A porous membrane separated the two compartments of the testing chamber. Up to four different fuel cells were tested simultaneously using this setup. A dissolved oxygen meter was used to continuously monitor the oxygen levels and temperature. A silver–silver chloride reference (Aldrich Double junction Ag/AgCl reference) electrode was used as the reference against which electrode potentials were measured.

4.2. Electrical testing setup

As illustrated in Fig. 4b, a Keithley 2400 Source-meter was used to apply a current sweep across the fuel cells and a Keithley 2000 Multi-meter equipped with a scanner card was used to take the voltage measurements of individual electrode potentials versus the reference electrode. The current sweep and channel switching was remotely controlled using a LABVIEW program. All current-potential characterization experiments were performed at a low sweep rate of $9\,\mu A\,h^{-1}$ in order to ensure that the readings were taken at a stable potential.

5. Experimental results

5.1. Electrode characterization experiments

Characterizing the individual performance of the cathode prior to integration in the fuel cell was carried out using a 3 elec-

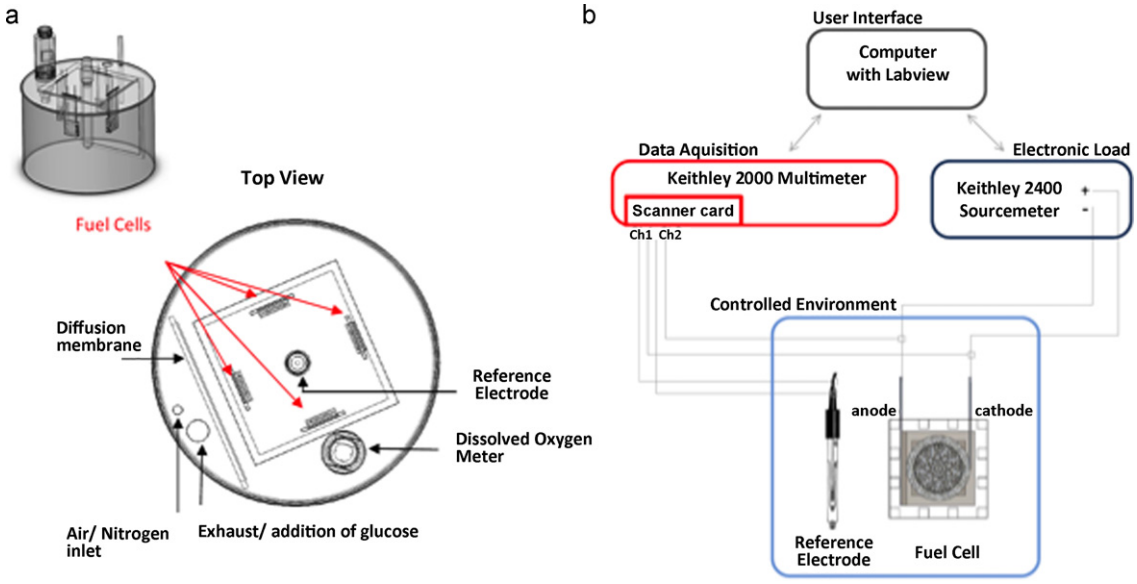

Fig. 4. (a) Controlled experiment set-up for fuel cell testing and (b) electrical testing set-up.

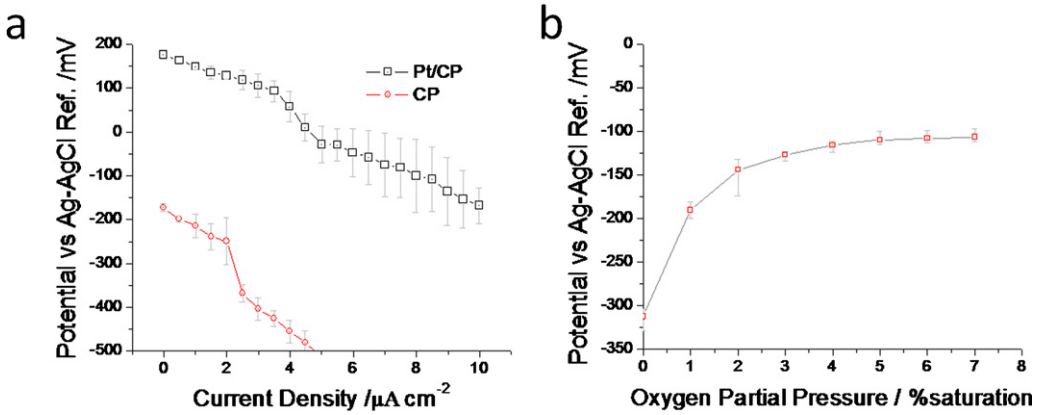

Fig. 5. (a) Potential versus current density plot for carbon paper (CP) and platinum on carbon paper (Pt/CP) cathodes and (b) effect of oxygen partial pressure on Pt/Ni electrode potential.

trode setup with a silver–silver chloride reference electrode and a carbon-paper auxiliary electrode. The potential versus current curves are shown in Fig. 5a for both the platinum on carbon paper electrode and the carbon paper electrode. A positive potential indicates that there is a cathodic current and that the oxygen reduction occurs as expected at the working electrode. It can be seen that the platinum on carbon paper electrode shows much better oxygen reduction potential than the carbon paper alone. The platinum on carbon paper electrode was prepared as described in Section 3.2 by sputtering 100 nm of Pt on both sides of the carbon paper. Preliminary experiments, not shown in this paper, with a higher amount of sputtered platinum on the carbon paper did not result in higher cathodic current, indicating that 100 nm is enough to fully coat the carbon paper with a catalyst layer. In addition, the open circuit voltage (OCV) of the electrode Platinum–Nickel electrodes against the Ag–AgCl reference electrode at different oxygen partial pressures is presented in Fig. 5b. It can be seen that due to the high reactivity of oxygen at the platinum surface, the OCV increases rapidly between 0% and 1% oxygen saturation. This demonstrates the necessity of fabricating the cathode in a way that minimizes the access of the oxygen to the anode.

5.2. Overall fuel cell performance

The overall performance of the glucose fuel cell with carbon paper supported cathode was characterized using the setup described in Section 4. Fig. 6a shows the cell potential and power density versus current density. The median value of three different experiments is indicated by the symbol and the error bars indicate the maximum and minimum experimental value. The peak power output for the cell is just under 2 $\mu W\,cm^{-2}$ and occurs at a current density of 15 $\mu A\,cm^{-2}$. Although the peak power output is lower than what has been reported by Kerzenmacher et al. [34] for mesh-free stacked fuel cells, the current density is much higher indicating better electrode kinetics. In addition, the fuel cell presented in this paper uses only 300 nm of platinum catalyst, over 100 times less than previous mesh-free designs, making it a relatively low-cost power source with a power density high enough for powering implantable sensor devices. Fig. 6b shows the power density of a fuel cell at a constant current density of 10 $\mu A\,cm^{-2}$ over a period of 4 h. A large initial drop in power density is observed due to the slow load change response of the fuel cell, however after a few minutes a stable power density of about 1.5 $\mu W\,cm^{-2}$ is reached. A power drop of less than 0.2 $\mu W\,cm^{-2}$ is observed over the next 4 h demonstrating that the carbon paper supported fuel cell is relatively stable at large current densities. The stable power density of 1.5 $\mu W\,cm^{-2}$ at 10 $\mu A\,cm^{-2}$ is consistent with the data presented for the polarization curve in Fig. 6a demonstrating that a sweep rate of 9 $\mu A\,h^{-1}$ did not lead to an overestimation of the performance.

5.3. Effect of inter-electrode gap and cathode thickness

The fuel cell presented in the previous sections had an inter-electrode gap size of 160 μm and a cathode thickness of 300 μm. As described in Section 2, it is expected that the gap between the electrodes to be an important factor determining fuel cell performance. In order to see the effect of the inter electrode gap on the maximum power output of the fuel cell, different gap thicknesses (50 μm,

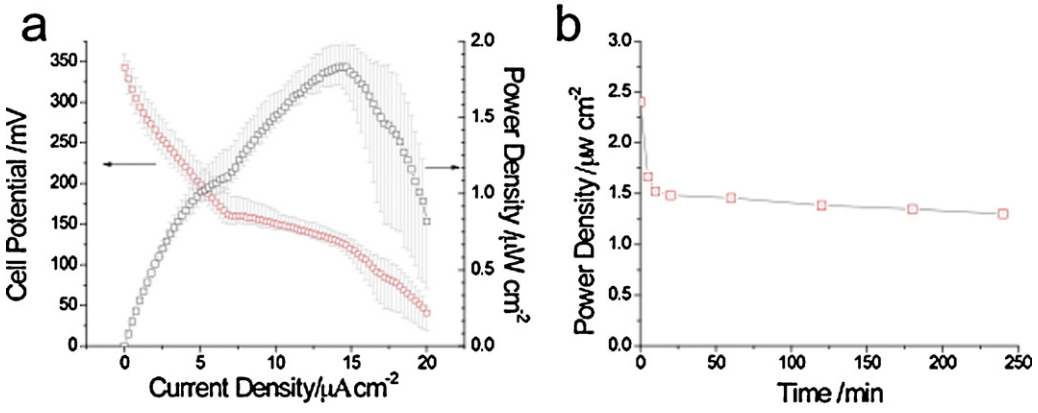

Fig. 6. (a) Dependence of cell voltage and power density on current density and (b) cell voltage versus time at 10 μW over a period of 4 h.

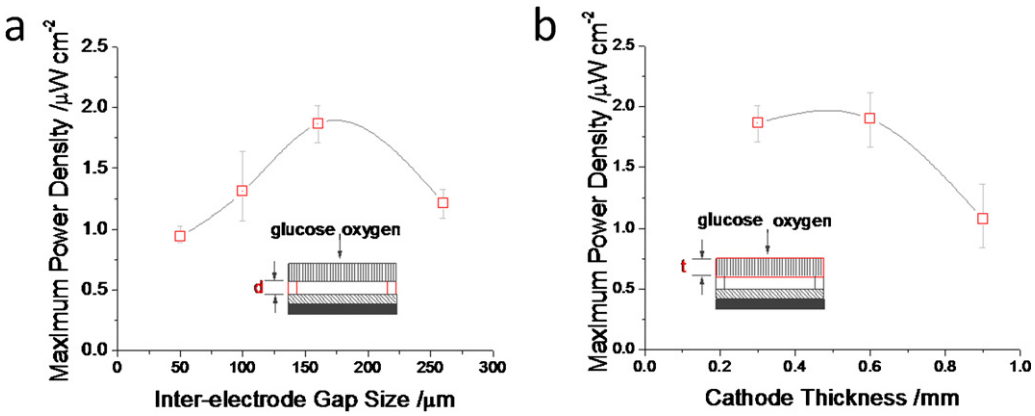

Fig. 7. (a) Effect of inter-electrode gap and (b) effect of electrode thickness on maximum power density.

100 μm, 160 μm and 260 μm) were patterned directly on the anode using SU-8 photoresist. The gap pattern was fabricated using standard photolithography techniques as described in Section 3 and the height of the pattern was measured using a P-10 Profilometer tool. Three fuel cells of each gap size were assembled and tested and the results are presented in Fig. 7a. It can be seen that the 160 μm gap electrode gave the maximum power density of 2 μW cm^{-2}. As mentioned is Section 2, the decrease in performance can be attributed to the change in concentration gradient at the anode as the gap size approaches the Nernst diffusion layer thickness. However, other effects such as hydrogen bubble formation at the anode and accumulation of reaction products at the electrode surface due to poor diffusivity through the membrane can also contribute to these observations.

The effect on cathode thickness on maximum power output is presented in Fig. 7b. The carbon paper used as a support for the platinum catalyst is 0.3 mm thick. Different cathode thicknesses were obtained by stacking 2 and 3 platinum on carbon paper electrodes and binding them with silver epoxy. Results indicate that a double stacked cathode performs better than the single electrode one but a sharp decrease in performance occurs for the triple stacked cathode. Although more oxygen reacts at the cathode when the thickness is increased, the diffusion of glucose to the anode appears to become the limiting factor.

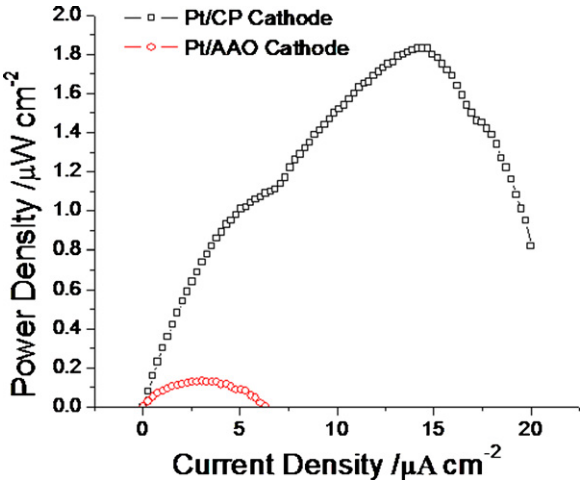

Fig. 8. Comparison between carbon paper (CP) and anodized aluminum oxide (AAO) cathode supports on fuel cell power output.

5.4. Comparison between different cathode supports

The performance of fuel cells with the cathode fabricated by sputtering platinum directly on a anodize aluminum oxide membrane was also measured. Fig. 8 shows the difference in power output between the two. It shows that everything else being identical during the fabrication, the carbon paper support gives a much better performance. The large difference in performance between the two can be explained by the much smaller cathode surface area obtained when a AAO membrane is used as cathode support. In addition, given that the membrane has a thickness of only 60 μm, compared to 300 μm for the carbon paper, it allows a larger amount of oxygen to diffuse through resulting in mixed-potential at the anode.

6. Conclusions

In this paper we have demonstrated the possibility of micromanufacturing enzyme-free glucose fuel cells without a filter membrane between the electrodes. This results in stacked fuel cells with lower ohmic resistance and better glucose diffusion to the anode. Compared to other designs the current fuel cell achieves much higher current densities [34]. We also demonstrate the advantage of using a conductive support such as carbon paper since it reduces the amount of platinum required for producing high surface area electrodes. The performance of platinum on carbon paper supported electrodes is much better than that of electrodes produced in a similar manner on anodized aluminum oxide membranes because of the higher surface area of the carbon paper. In previous studies, in order to fabricate the cathode, either a hydrogel was used to support the catalyst materials [29] or a silicon wafer with etched holes was used as a substrate for the deposition of the cathodic layer [30]. The first method has the drawback of producing thick electrodes and having limited stability against hydrolytic and oxidative attack while the latter approach requires numerous fabrication steps and a thick platinum catalyst layer for the formation of a high surface area Raney type catalyst layer. The carbon paper support allows for the fabrication of thinner and more stable electrodes which results in better glucose diffusivity through the cathode as indicated by the higher power density. It was shown that a peak power density of 2 μW cm^{-2} occurs when the inter-electrode spacing is about 160 μm. At large inter-electrode spacing the peak power density is lower due to higher ohmic losses, while at smaller inter-electrode spacing the decrease in performance can be attributed to the change in concentration gradient at the anode as the gap size approaches the Nernst diffusion layer thickness. A small increase in performance was observed as the cathode thickness was increased from 300 μm to 600 μm but a sharp decrease was

observed as the thickness was further increased. This shows that although a thicker electrode allows for better oxygen–glucose separation, the decrease in diffusivity of glucose to the anode becomes the limiting factor.

Acknowledgments

The authors wish to acknowledge the support of the Office of Naval Research (ONR). In addition one of the authors (V.O.) wishes to acknowledge the support of the Canadian institutions FQRNT and NSERC through fellowships. The fabrication steps described in this paper were carried out at the Cornell Nanoscale Facility (CNF) and the Nanobiotechnology Center at Cornell University (NBTC). The XPS analysis was performed by John Shu at the Cornell Center for Material Research (CCMR).

References

[1] C.A. Vincent, Solid State Ionics 134 (1–2) (2000) 159–167.
[2] S. Roundy, P.K. Wright, J. Rabaey, Comput. Commun. 26 (11) (2003) 1131–1144.
[3] E. Jalilian, et al., Med. Eng. Phys. 29 (2) (2007) 238–252.
[4] A.S. Jurkov, A. Arriagada, M.P. Mintchev, Engineering in Medicine and Biology Society, 2009, EMBC 2009. Annual International Conference of the IEEE, 2009.
[5] H. Ebel, et al., Acta Neurochir. 138 (11) (1996) 1300–1306.
[6] M.T. Salam, M. Sawan, D.K. Nguyen, Engineering in Medicine and Biology Society (EMBC), 2010, Annual International Conference of the IEEE, 2010.
[7] P.A. Federspil, P.K. Plinkert, Biomed. Tech. 49 (4) (2004) 78–82.
[8] S. Vaddiraju, et al., Biosens. Bioelectron. 25 (7) (2010) 1553–1565.
[9] A.J. Chung, D. Kim, D. Erickson, Lab Chip 8 (2) (2008) 330–338.
[10] S. Zafar Razzacki, et al., Adv. Drug Deliv. Rev. 56 (2) (2004) 185–198.
[11] J. Gyu Bum, B.H. Cho, Power Electron. IEEE Trans. 13 (6) (1998) 1013–1022.
[12] H. Miura, et al., Magn. IEEE Trans. 42 (10) (2006) 3578–3580.
[13] F. Davis, S.P.J. Higson, Biosens. Bioelectron. 22 (7) (2007) 1224–1235.
[14] S.D. Minteer, B.Y. Liaw, M.J. Cooney, Curr. Opin. Biotechnol. 18 (3) (2007) 228–234.
[15] B.E. Logan, et al., Environ. Sci. Technol. 40 (17) (2006) 5181–5192.
[16] R.A. Bullen, et al., Biosens. Bioelectron. 21 (11) (2006) 2015–2045.
[17] S. Kerzenmacher, et al., J. Power Sources 182 (1) (2008) 1–17.
[18] Y. Yang, et al., J. Phys. D: Appl. Phys. 40 (18) (2007) 5790.
[19] Z.L. Wang, J. Song, Science 312 (5771) (2006) 242–246.
[20] K.A. Cook-Chennault, et al., Smart Mater. Struct. 17 (4) (2008) 043001.
[21] P.X. Gao, et al., Adv. Mater. 19 (1) (2007) 67–72.
[22] S. Kerzenmacher, et al., Solid-State Sensors, Actuators and Microsystems Conference, 2007, TRANSDUCERS 2007 International, 2007.
[23] J.R. Rao, G. Richter, Naturwissenschaften 61 (5) (1974) 200–206.
[24] R.F. Drake, et al., Trans. – Am. Soc. Artif. Intern. Organs 16 (1970) 199–205.
[25] N. Mano, F. Mao, A. Heller, J. Am. Chem. Soc. 125 (21) (2003) 6588–6594.
[26] S. Calabrese Barton, J. Gallaway, P. Atanassov, Chem. Rev. 104 (10) (2004) 4867–4886.
[27] S.K. Chaudhuri, D.R. Lovley, Nat. Biotechnol. 21 (10) (2003) 1229–1232.
[28] K. Rabaey, et al., Biotechnol. Lett. 25 (18) (2003) 1531–1535.
[29] S. Kerzenmacher, et al., J. Power Sources 182 (1) (2008) 66–75.
[30] S. Kerzenmacher, et al., J. Power Sources 196 (3) (2011) 1264–1272.
[31] U. Gebhardt, J.R. Rao, G.J. Richter, J. Appl. Electrochem. 6 (2) (1976) 127–134.
[32] N. Nagai, et al., Int. J. Hydrogen Energy 28 (1) (2003) 35–41.
[33] Y.B. Vassilyev, O.A. Khazova, N.N. Nikolaeva, J. Electroanal. Chem. Interfacial Electrochem. 196 (1) (1985) 105–125.
[34] S. Kerzenmacher, et al., in: J. Sloten, et al. (Eds.), 4th European Conference of the International Federation for Medical and Biological Engineering, Springer, Berlin/Heidelberg, 2009, pp. 2379–2383.